INU
I-65

Inorganic Chemistry

including bioinorganic chemistry

November 4, 2013
Volume 52, Number 21
pubs.acs.org/IC

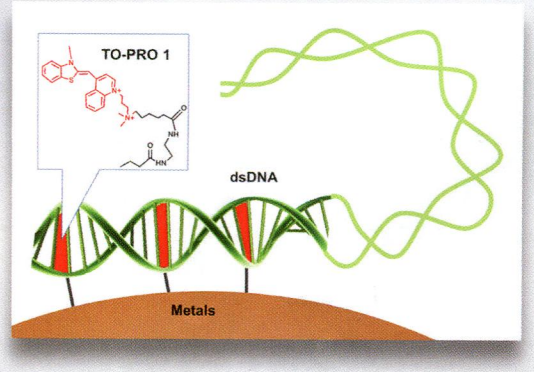

Forum on Metals in Medicine and Health

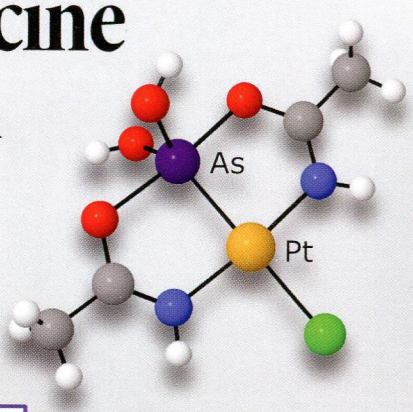

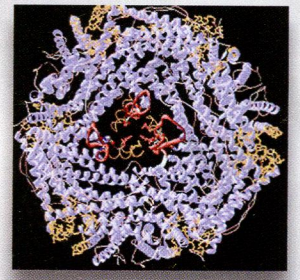

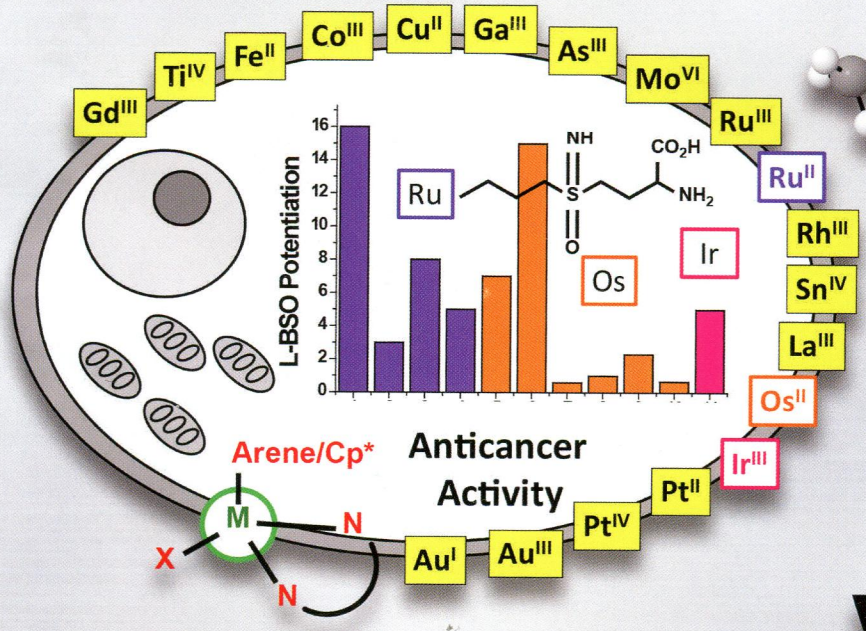

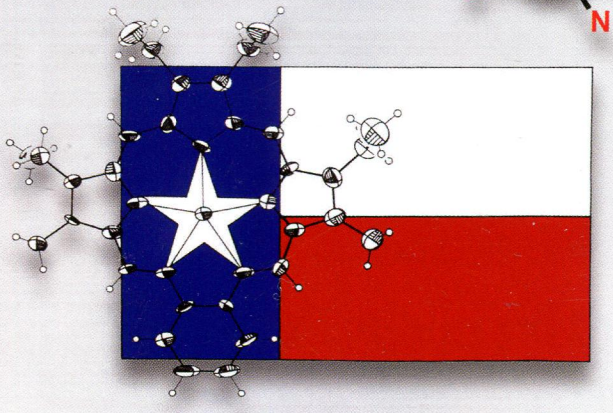

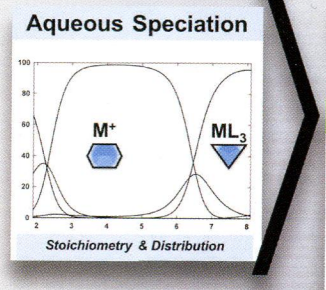

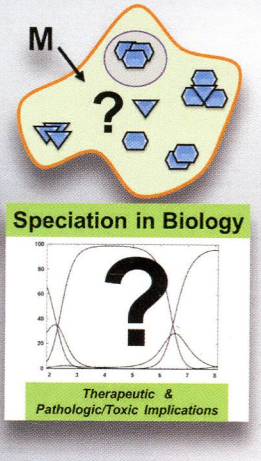

ACS Publications
MOST TRUSTED. MOST CITED. MOST READ.

www.acs.org

Inorganic Chemistry

NOVEMBER 4, 2013
VOLUME 52 ISSUE 21

INOCAJ 52(21) 12181−12854 (2013)
ISSN 0020-1669
Registered in the U.S. Patent and Trademark Office
© 2013 by the American Chemical Society

ON THE COVER: The significant growth in the area of Metals in Medicine and Health is represented by a series of research contributions embracing metal-based diagnostics and drugs. This area of research naturally reaches across the aisles of many disciplines, with advances in inorganic coordination chemistry driving the growth in drug discovery teams in industry and academia embracing nontraditional approaches for translation of drugs into clinical medicine.

Forum on Metals in Medicine and Health: New Opportunities and Approaches to Improving Health

Forum Articles

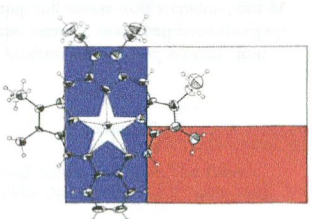

12193 dx.doi.org/10.1021/ic4003059

Role of Metal Ions in the Self-assembly of the Alzheimer's Amyloid-β Peptide

Peter Faller,* Christelle Hureau, and Olivia Berthoumieu

Metal ions, particularly zinc and copper, are enriched in certain synapses, where they are ejected, being transient in high local concentrations. These metal ions seem to play a role in the aggregation of peptide amyloid-β (Aβ) into senile plaques, a key process in Alzheimer's disease, because they can bind to Aβ and modulate the aggregation process. The present review focuses on the role of Zn^{II} and Cu in Aβ aggregation.

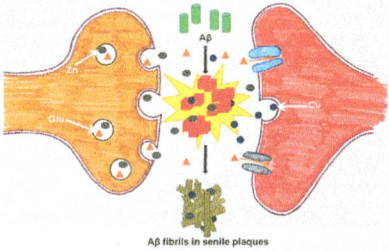

12207 S dx.doi.org/10.1021/ic400295f

Metalloprotein–Inhibitor Binding: Human Carbonic Anhydrase II as a Model for Probing Metal–Ligand Interactions in a Metalloprotein Active Site

David P. Martin, Zachary S. Hann, and Seth M. Cohen*

Human carbonic anhydrase II (hCAII), a zinc(II)-dependent hydrolase, has been widely studied to understand ligand–protein binding such as hydrogen-bonding and hydrophobic interactions. This report expands the use of hCAII as a model system by examining how ligand binding is effected by mutations of residues within the zinc(II)-ion coordination sphere. In this way, we can begin to understand how metal-binding group selectivity and affinity is perturbed by the composition of the ligating active-site residues.

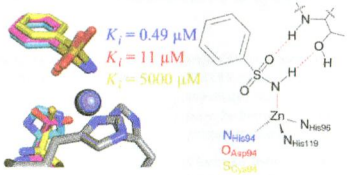

12216 dx.doi.org/10.1021/ic400404g

Imaging DNA with Fluorochrome Bearing Metals

Hoonsung Cho, Yanyan Guo, David E. Sosnovik, and Lee Josephson*

DNA is an important mediator of dead cell clearance, coagulation reactions, and an immunogen in autoimmune lupus. We describe the use of a DNA-binding fluorochrome, TO-PRO 1, as a targeting vehicle for metals that allow DNA imaging by whole-body-imaging modalities by magnetic resonance imaging and, potentially, by single-photon emission computerized tomography or positron emission tomography. These "metal-bearing" fluorochromes retain their ability to fluorescence upon binding DNA, while being detectable through the presence of their metal by a whole-body-imaging modality.

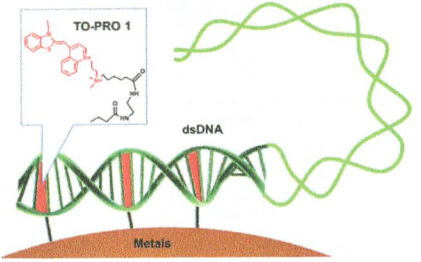

12223 dx.doi.org/10.1021/ic400484n

Ferritin: The Protein Nanocage and Iron Biomineral in Health and in Disease

Elizabeth C. Theil*

Ferritin protein cages and iron biominerals are described. Possible targets in ferritin protein−protein and protein−iron interactions for therapeutic development in modulate disease are indicated, such as the catalytic sites (pathogen-specific), folded ferritin pores (improved iron chelation), the ferritin mRNA riboregulator (stabilizing excess iron accumulations in hypertransfusion therapies), and protein cage assembly (nanodrug/nanosensor delivery).

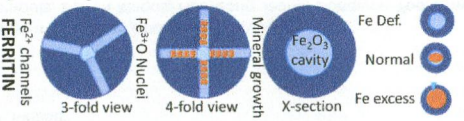

12234 S dx.doi.org/10.1021/ic400538c

Monofunctional and Higher-Valent Platinum Anticancer Agents

Timothy C. Johnstone, Justin J. Wilson, and Stephen J. Lippard*

A discussion of the recent developments from our laboratory in the areas of platinum(II) monofunctional compounds, platinum(IV) prodrugs, and nanodelivery of platinum(IV) complexes.

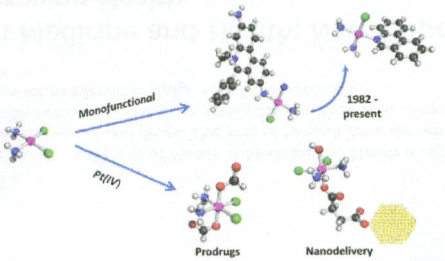

12250 S dx.doi.org/10.1021/ic400681j

Structural Optimization of Zn(II)-Activated Magnetic Resonance Imaging Probes

Lauren M. Matosziuk, Jonathan H. Leibowitz, Marie C. Heffern, Keith W. MacRenaris, Mark A. Ratner,* and Thomas J. Meade*

Through systematic structural modifications to the Zn(II)-activated contrast agent, Gd-*n*, the change in relaxivity upon the addition of Zn(II) was optimized. Moreover, specific structural characteristics required for effective water restriction in *q*-modulated magnetic resonance contrast agents were elucidated.

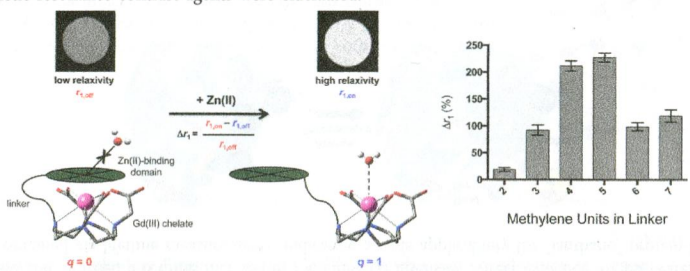

12262 dx.doi.org/10.1021/ic4007873

Metal Speciation in Health and Medicine Represented by Iron and Vanadium

Debbie C. Crans,* Kellie A. Woll, Kestutis Prusinskas, Michael D. Johnson, and Eugenijus Norkus

The coordination chemistry of metal compounds and their speciation distribution has a profound effect on biology, ranging from metal uptake to beneficial or detrimental interactions with the metalloproteins. The systems of some metals are tightly regulated, whereas others can form a range of species. Knowing and understanding the speciation and coordination chemistry of these systems can be advantageous and may result in the treatment of diseases.

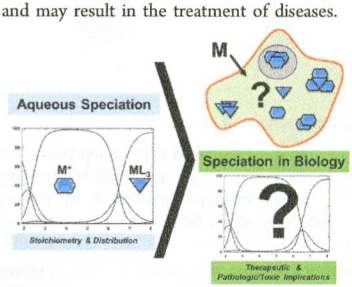

12276 Ⓢ dx.doi.org/10.1021/ic400835n

Next-Generation Metal Anticancer Complexes: Multitargeting via Redox Modulation

Isolda Romero-Canelón and Peter J. Sadler*

New generations of metal complexes are needed to circumvent resistance, side effects, and the limited spectrum of activity of platinum drugs. We highlight metal-based anticancer agents with potential redox mechanisms of action. Targeting the redox balance in cancer cells may be a highly effective strategy for cancer treatment, a multiple-site approach offering selectivity over normal cells. We show how redox modulation increases the potency of organometallic ruthenium(II) and osmium(II) arene and iridium(III) cyclopentadienyl complexes to nanomolar levels.

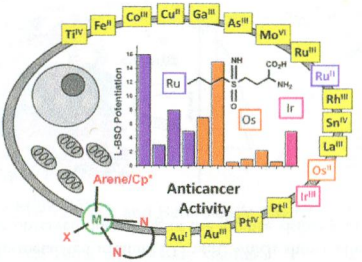

12292 dx.doi.org/10.1021/ic401211u

Anticancer Activity of Small-Molecule and Nanoparticulate Arsenic(III) Complexes

Elden P. Swindell, Patrick L. Hankins, Haimei Chen, Đenana U. Miodragović, and Thomas V. O'Halloran*

Arsenic compounds have been used in the treatment of disease since Chinese and Greek antiquity. Modern interest in therapeutic arsenicals has been driven by the discovery that low doses of arsenic trioxide lead to complete remission of certain types of leukemia. This Forum Article discusses arsenic biochemistry, metabolism, and toxicity and how they relate to the anticancer use of arsenic. Additionally, we discuss novel arsenical drugs and how they may alleviate the side effects of arsenic treatment.

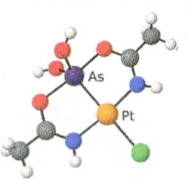

Communications

12305 Ⓢ dx.doi.org/10.1021/ic400824f

Unusual C–S Bond Cleavage in Hydro(solvo)thermal Reaction That Induces Two Novel Nickel Thiolates: The Crown $[Ni_{16}(edt)_8S_9(S_2)]^{4-}$ with an Unprecedented 12-Membered Ring System and the Cagelike $[Ni_{13}(edt)_8S_4(S_2)_2]^{2-}$ with Two Distorted Cores

Hao Jiang, Tianlu Sheng, Songyan Bai, Shengmin Hu, Xin Wang, Ruibiao Fu, Peng Yu, and Xintao Wu*

Two fascinating anion clusters, $[Ni_{16}(edt)_8S_9(S_2)]^{4-}$ (**1**) and $[Ni_{13}(edt)_8S_4(S_2)_2]^{2-}$ (**2**), where edt = 1,2-ethanedithiol, have been successfully directed in hydro(solvo)thermal conditions. **1** exhibits a crown structure with unprecedented 12-membered rings. Meanwhile, **2** is a cagelike cluster with two distorted cores. Interestingly, the two novel compounds were first synthesized by way of C–S cleavage from an acyclic thiol in the field of nickel thiolates.

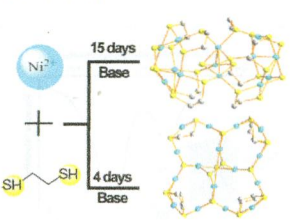

12308 S dx.doi.org/10.1021/ic402436w

Observation of Room Temperature B–Cl Activation of the $HCB_{11}Cl_{11}^-$ Anion and Isolation of a Stable Anionic Carboranyl Phosphazide

Allen L. Chan, Javier Fajardo Jr., James H. Wright II, Matthew Asay, and Vincent Lavallo*

When the $HCB_{11}Cl_{11}$ anion is treated with base and subsequently reacted with tosyl azide, two competing reactions are observed. The minor reaction pathway is an unprecedented B–Cl activation/cycloaddition at ambient temperature. The dominant pathway leads to the formation of a perchlorinated carba-*closo*-dodecaborate azide $N_3CB_{11}Cl_{11}$. This azide reacts readily with PPh_3 to afford a stable anionic lithium phosphazide complex.

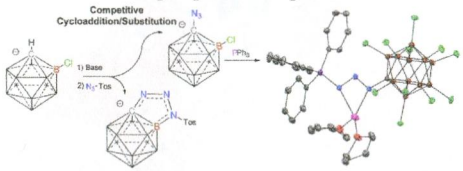

12311 S dx.doi.org/10.1021/ic401571h

Measurement of the Md^{3+}/Md^{2+} Reduction Potential Studied with Flow Electrolytic Chromatography

Atsushi Toyoshima,* Zijie Li, Masato Asai, Nozomi Sato, Tetsuya K. Sato, Takahiro Kikuchi, Yusuke Kaneya, Yoshihiro Kitatsuji, Kazuaki Tsukada, Yuichiro Nagame, Matthias Schädel, Kazuhiro Ooe, Yoshitaka Kasamatsu, Atsushi Shinohara, Hiromitsu Haba, and Julia Even

The reduction behavior of mendelevium (Md) was studied using a flow electrolytic chromatography apparatus. By application of the appropriate potentials on the chromatography column, the more stable Md^{3+} is reduced to Md^{2+}. The reduction potential of the $Md^{3+} + e^- \rightarrow Md^{2+}$ couple was determined to be -0.16 ± 0.05 V versus a normal hydrogen electrode.

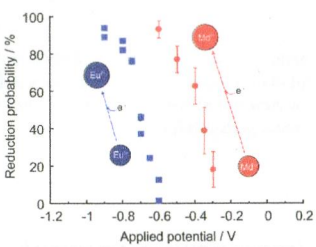

12314 S dx.doi.org/10.1021/ic4018932

Smart "Lanthano" Proteins for Phospholipid Sensing

Shafali Gupta, Samsuzzoha Mondal, Amit Mhamane, and Ankona Datta*

"Turn-on" lanthanide reconstituted-protein sensors have been designed based on the displacement of inner-sphere water molecules on metal sites by anionic phospholipids. A "lanthano" annexin V based optical sensor responded selectively to phosphatidylserine and afforded a 6 times increase in the emission intensity. Direct evidence for the water-displacement mechanism was obtained via lifetime measurements, indicating a wide applicability for "lanthano"-protein-based sensors in lipid sensing.

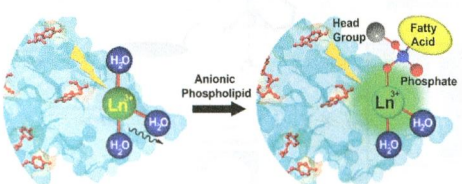

12317 S

dx.doi.org/10.1021/ic4021492

Mixed-Valent Neptunium(IV/V) Compound with Cation–Cation-Bound Six-Membered Neptunyl Rings

Geng Bang Jin*

$Na_xNp^{IV}(Np^{V}O_2)_6(OH)_{1+x}Cl_9(H_2O)_{8-x}$ $(0 < x \leq 1)$ has been synthesized by evaporation of a neptunium(V) acidic solution. Its structure contains cation–cation-bound six-membered neptunyl(V) rings, which are further connected by Np^{IV} ions through cation–cation interactions (CCIs) into a three-dimensional neptunium cationic open framework. The formation of this compound exemplifies the possibility of isolating neptunyl(V) CCI oligomers in inorganic systems and provides insight into the disproportionation reaction of Np^{V} ions.

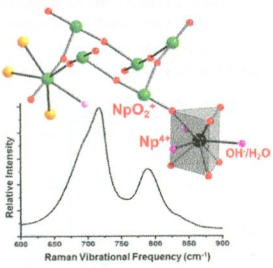

12320 S

dx.doi.org/10.1021/ic402155h

Dimeric and Tetrameric Supramolecular Aggregates of Single-Molecule Magnets via Carboxylate Substitution

Andrew M. Mowson, Tu N. Nguyen, Khalil A. Abboud, and George Christou*

$[Mn_3]_2$ and $[Mn_3]_4$ supramolecular aggregates of weakly exchange-coupled Mn^{III}_3 single-molecule magnets (SMMs) with $S = 6$ have been prepared by carboxylate substitution on the preformed Mn_3 acetate monomer using the dicarboxylic acids α-truxillic acid and fumaric acid, respectively. The method opens up a new approach to Mn_3 SMM aggregates of various size and topology.

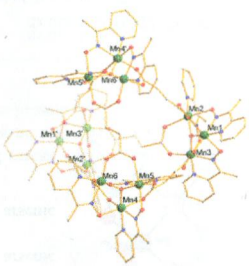

12323 S

dx.doi.org/10.1021/ic402158n

An Intensely Luminescent Metal–Organic Framework Based on a Highly Light-Harvesting Dyclo-Metalated Iridium(III) Unit Showing Effective Detection of Explosives

Lina Li, Shuquan Zhang, Liangjin Xu, Liang Han, Zhong-Ning Chen, and Junhua Luo*

A rare intensely luminescent metal–organic framework with long lifetime and enhanced quantum yield has been obtained based on a highly light-harvesting dyclo-metalated iridium(III) unit, which shows effective detection of nitroaromatic explosives on the ppm scale. The ocular observed quenching of the intense visible yellow-orange emission make **1** convenient and sensitive to trace the nitroaromatic explosives.

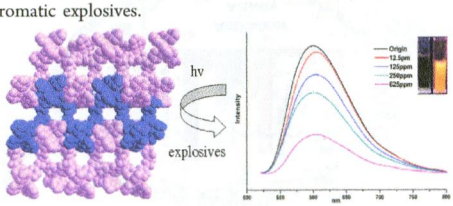

12326 S dx.doi.org/10.1021/ic402241f

Unprecedented Nitronyl Nitroxide Bridged 3d–4f Complexes: Structure and Magnetic Properties

Mei Zhu, Yun-Gai Li, Yue Ma, Li-Cun Li,* and Dai-Zheng Liao

Two unprecedented two-dimensional 2p–3d–4f complexes have been synthesized by using the nitronyl nitroxide radical with nonchelating N donor atoms. The compounds have a unique topological architecture type that consists of a two-dimensional network with alternating cyclic $[Cu_2]$ dimer rings and rectangle-like $[Cu_4Ln_2]$ rings. Ferromagnetic behaviors were observed in both compounds.

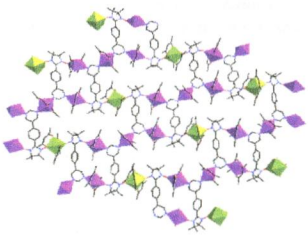

12329 S dx.doi.org/10.1021/ic402257z

Noninnocent Behavior of Bidentate Amidophosphido $[NP]^{2-}$ Ligands upon Coordination to Copper

Mark W. Bezpalko, Bruce M. Foxman, and Christine M. Thomas*

A new class of bidentate ligands featuring an amidophosphido donor set has been developed and investigated for potential noninnocent behavior. Treatment with copper(II) leads to ligand oxidation, and the resulting ligand-based radical intermolecularly couples to form a dicopper(I) complex bridged by a P–P linkage.

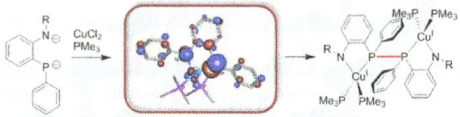

12332 S dx.doi.org/10.1021/ic4022992

Directed Formation of a Ferrocenyl-Decorated Organotin Sulfide Complex and Its Controlled Degradation

Zhiliang You and Stefanie Dehnen*

Attachment of ferrocenyl (Fc) units to an organo-functionalized precursor yielded the Fc-decorated complex $[(R^{Fc}Sn)_4Sn_6S_{10}]$ [**1**; $R^{Fc} = CMe_2CH_2C(Me)=N-N=C(Me)Fc$]. Electronic interaction between the Fc units has been studied using cyclic and differential pulse voltammetry. The addition of different amounts of hydrochloric acid to a solution of **1** produced the derivatives $[(R^{Fc}SnCl_2)_2S]$ (**2**) and $[R^{Fc}SnCl_3{\cdot}HCl]$ (**3**), the latter of which acts as a precursor to the formation/recovery of **2** or **1**, respectively.

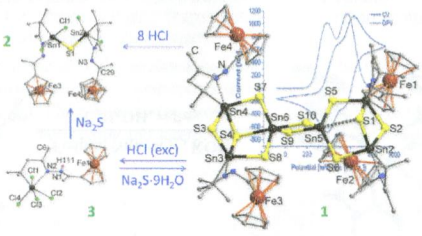

12335 S dx.doi.org/10.1021/ic402517m

Reductive Coupling of Azides Mediated by an Iron(II) Bis(alkoxide) Complex

James A. Bellow, Philip D. Martin, Richard L. Lord,* and Stanislav Groysman*

Unexpected reductive coupling of an azide was observed at the iron(II) center featuring a bis(alkoxide) ligand environment. Density functional theory calculations suggest intermediacy of an iron azide dimer on the route to the coupled hexazene product, in which each azide is monoreduced and the iron centers are oxidized to the 3+ oxidation state.

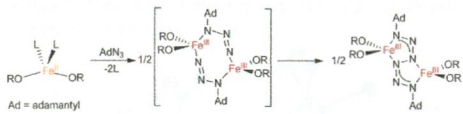

Articles

12338 S dx.doi.org/10.1021/ic400950u

Photophysical Properties of Substituted Homoleptic and Heteroleptic Phenylimidazolinato Ir(III) Complexes as a Blue Phosphorescent Material

Takashi Karatsu,* Masatomo Takahashi, Shiki Yagai, and Akihide Kitamura

Blue phosphorescent homoleptic and heteroleptic iridium(III) tris(phenylimidazolinate) complexes were synthesized. DFT calculation showed that the HOMO localized at the iridium d- and phenyl π-orbitals. The LUMO is also localized on the phenyl moiety with a high population. This LUMO character is different from other typical blue and green phosphorescent complexes. Therefore, substitution with π-electron donating and electron withdrawing groups induces blue and red spectral shifts, respectively, which is the reverse shift exhibited by other complexes.

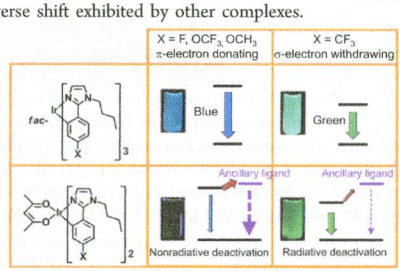

12351 S

dx.doi.org/10.1021/ic401099c

Synthesis, Spectral, and Structural Studies of Porphyrins Having Sterically Hindered [η^5-CpCo(η^4-C_4Ph_4)] Cobalt Sandwich Units at the Meso Positions

Karunesh Keshav, Dheeraj Kumar, and Anil J. Elias*

The synthesis and structural characterization of the first examples of porphyrins substituted at the *meso* positions with sterically hindered η^5-CpCo(η^4-C_4Ph_4) cobalt sandwich units are described. The synthesis of these porphyrins were made possible by the facile preparation of the first dipyrromethane derivative of (η^5-Cp)Co(η^4-C_4Ph_4) and its 1,9-diformyl derivative. The new porphyrins consisting of metal complexed and free base porphyrins with mono- and disubstitution of η^5-CpCo(η^4-C_4Ph_4) at the periphery have been prepared by rational methods and characterized by a variety of spectral, electrochemical, and structural studies.

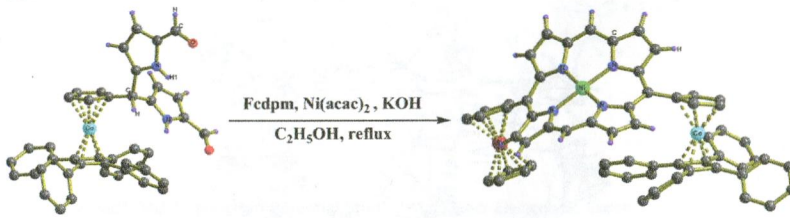

12367 S

dx.doi.org/10.1021/ic402092r

Mild Solvothermal Syntheses of Thioargentates A–Ag–S (A = K, Rb, Cs) and A–Ag–Ge–S (A = Na, Rb): Crucial Role of Excess Sulfur

Chi Zhang, Kai-Ni Wang, Min Ji, and Yong-Lin An*

A novel layered compound, $Na_5AgGe_2S_7$, in which a dimeric $[Ge_2S_7]^{6-}$ cluster forms part of the bonding network has been solvothermally synthesized under mild conditions in the presence of excess sulfur as a mineralizer.

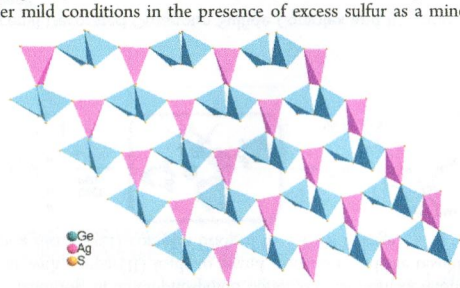

12372 S dx.doi.org/10.1021/ic401201w

Solid State Complex Chemistry: Formation, Structure, and Properties of Homoleptic Tetracyanamidogermanates $RbRE[Ge(CN_2)_4]$ (RE = La, Pr, Nd, Gd)

Markus Kalmutzki, David Enseling, John E. C. Wren, Scott Kroeker, Victor V. Terskikh, Thomas Jüstel, and H.-Jürgen Meyer*

Homoleptic tetracyanamidogermanates were prepared via exothermic solid state metathesis reactions under thermoanalytical control. The products were characterized as $RbRE[Ge(CN_2)_4]$ (RE = La, Pr, Nd, Gd) by powder XRD, IR, and solid state NMR measurements. Luminescence properties of doped samples are reported.

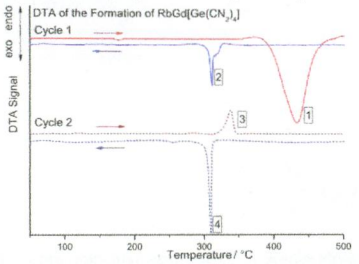

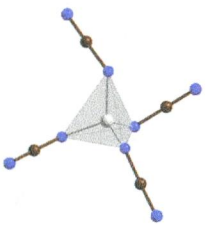

12383 S dx.doi.org/10.1021/ic401234t

Synthesis and Structural Characterization of a Series of $Mn^{III}OR$ Complexes, Including a Water-Soluble $Mn^{III}OH$ That Promotes Aerobic Hydrogen-Atom Transfer

Michael K. Coggins, Lisa M. Brines, and Julie A. Kovacs*

The synthesis, structure, and reactivity properties of a series of $Mn^{III}OR$ compounds [R = $^{p}NO_2Ph$ (**5**), Ph (**6**), Me (**7**), H (**8**)], including a rare example of a mononuclear $Mn^{III}OH$ complex **8**, are reported. Complex **8** is water-soluble with a pH-dependent redox potential consistent with $1H^{+}/1e^{-}$ proton-coupled electron-transfer. Despite their mild redox potentials, **7** and **8** each react with TEMPOH with k_H/k_D values consistent with concerted H-atom abstraction. The thiolate is proposed to contribute to this reactivity by increasing the basicity of the bound oxygen.

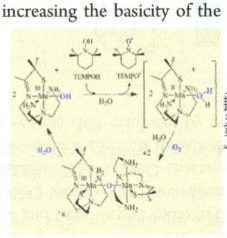

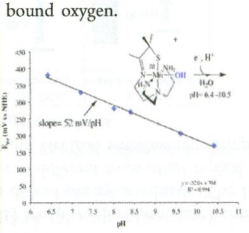

12394 S dx.doi.org/10.1021/ic4012444

Synthesis, Structures, and Properties of Uranyl Hybrids Constructed by a Variety of Mono- and Polycarboxylic Acids

Weiting Yang, Song Dang, Hao Wang, Tao Tian, Qing-Jiang Pan, and Zhong-Ming Sun*

A series of uranyl coordination materials with various structures have been hydrothermally synthesized by using various organic ligands. Compounds **1**, **7**, and **8** feature one-dimensional arrangements, **2** and **3** are present as layered structures, and **4**–**6** are molecular assemblies.

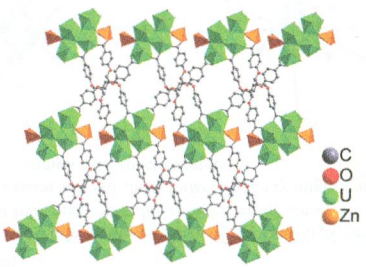

12403 S dx.doi.org/10.1021/ic4011532

Photophysical Properties of Cyclometalated Pt(II) Complexes: Counterintuitive Blue Shift in Emission with an Expanded Ligand π System

Alberto Bossi, Andreas F. Rausch, Markus J. Leitl, Rafał Czerwieniec, Matthew T. Whited, Peter I. Djurovich, Hartmut Yersin,* and Mark E. Thompson*

The photophysical properties of three cyclometalated Pt(II) complexes were examined in detail. A derivative with an expanded aromatic π-system displays a counterintuitive blue shift in its phosphorescence spectrum.

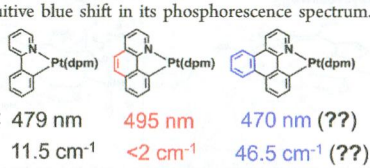

12416 S dx.doi.org/10.1021/ic401208p

Palladium-Catalyzed Direct Arylation of Luminescent Bis-Cyclometalated Iridium(III) Complexes Incorporating *C^N*- or *O^O*-Coordinating Thiophene-Based Ligands: an Efficient Method for Color Tuning

Kassem Beydoun, Moussa Zaarour, J. A. Gareth Williams, Thierry Roisnel, Vincent Dorcet, Aurélien Planchat, Abdou Boucekkine, Denis Jacquemin,* Henri Doucet,* and Véronique Guerchais*

The palladium-catalyzed direct 5-arylation of both metalated and nonmetalated thiophene moieties of iridium complexes with aryl halides via C–H bond functionalization opens new routes to varieties of Ir complexes in only one step, allowing easy modification of the nature of the ligand. The photophysical properties of the new functionalized complexes have been studied by means of absorption and emission spectroscopy and interpreted with the help of time-dependent density functional theory (TD-DFT) calculations.

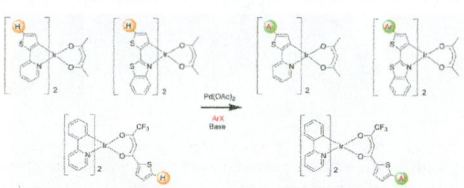

12429 dx.doi.org/10.1021/ic4012923

Alkaline Earth Complexes of Silylated Aminopyridinato Ligands: Homoleptic Compounds and Heterobimetallic Coordination Polymers

Fabrizio Ortu, Graeme J. Moxey, Alexander J. Blake, William Lewis, and Deborah L. Kays*

Sterically demanding aminopyridinato ligands have been used to stabilize magnesium and calcium complexes, including the first structurally characterized homoleptic calcium aminopyridinato complex and heterobimetallic calciate species, the first supported by a bidentate *N*-donor ligand. These ligands also support $[(\mathbf{L^1})\mathrm{Li}(\mu_2\text{-}^n\mathrm{Bu})\mathrm{Mg}(\mathbf{L^1})]_\infty$, the first complex to feature an unsupported bridging butyl interaction between two metals.

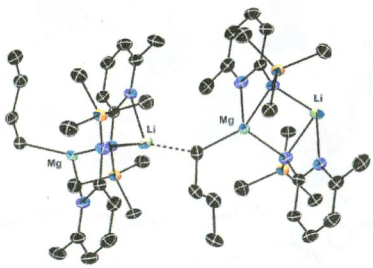

12440 dx.doi.org/10.1021/ic401362s

Synthesis, Characterization, and Anticancer Activity of a Series of Ketone-N^4-Substituted Thiosemicarbazones and Their Ruthenium(II) Arene Complexes

Wei Su,* Quanquan Qian, Peiyuan Li,* Xiaolin Lei, Qi Xiao, Shan Huang, Chusheng Huang, and Jianguo Cui

A series of ketone-N^4-substituted thiosemicarbazone (TSC) compounds (**L1**–**L9**) and their corresponding $[(\eta^6\text{-}p\text{-cymene})\mathrm{Ru^{II}}(\mathrm{TSC})\mathrm{Cl}]^{+/0}$ complexes (**1**–**9**) were synthesized and characterized by NMR, IR, elemental analysis, and HR-ESI-mass spectrometry.

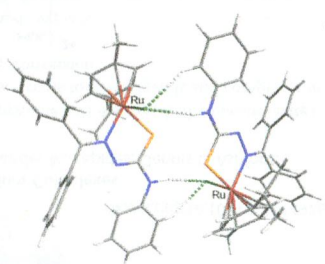

12450 dx.doi.org/10.1021/ic401437r

Anion and Solvent Induced Chirality Inversion in Macrocyclic Lanthanide Complexes

Aleksandra Gerus, Katarzyna Ślepokura, and Jerzy Lisowski*

The helical conformation of a chiral hexaaza macrocycle can be inverted by addition of achiral nitrate anions to the chloride derivatives of macrocyclic lanthanide(III) complexes. This process is accompanied by the change of chirality at the stereogenic nitrogen atoms and rearrangement of the axial ligands at the two sides of the macrocycle.

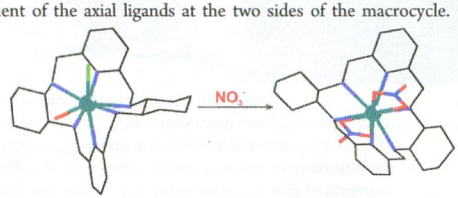

12461 S dx.doi.org/10.1021/ic4014619

Complex 5d Magnetism in a Novel $S = 1/2$ Trimer System, the 12L Hexagonal Perovskite $Ba_4BiIr_3O_{12}$

Wojciech Miiller, Matthew T. Dunstan, Zixin Huang, Zakiah Mohamed, Brendan J. Kennedy, Maxim Avdeev, and Chris D. Ling*

$Ba_4BiIr_3O_{12}$ consists of Ir_3O_{12} linear face-sharing octahedral trimer units bridged by corner-sharing BiO_6 octahedra. Antiferromagnetic coupling among $S = 1/2$ Ir^{4+} (d^5) cations leads to the formation of $S = 1/2$ doublets within the trimers. The onset of magnetic order is accompanied by anomalies in magnetic susceptibility, heat capacity, electrical resistivity, and unit cell parameters; however, long-range magnetic order is not observed because interactions between the trimers are geometrically frustrated.

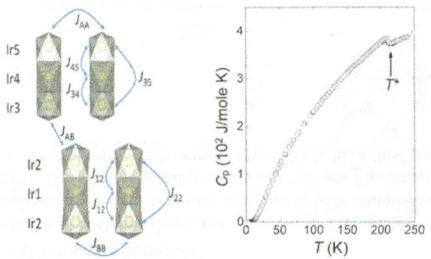

12468 S dx.doi.org/10.1021/ic401467k

Studies of Iron(III) Porphyrinates Containing Silanethiolate Ligands

Daniel J. Meininger, Jonathan D. Caranto, Hadi D. Arman, and Zachary J. Tonzetich*

The preparation, characterization, and reactivity of iron(III) porphyrinates containing silanethiolate ligands is presented.

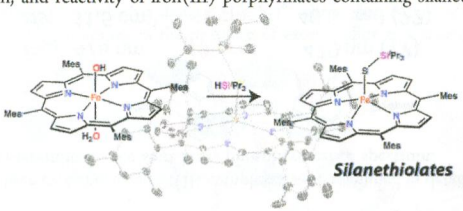

12477 S dx.doi.org/10.1021/ic401377g

Alkynyl Complexes of High-Valence Clusters. Synthesis and Luminescence Properties of $[Mo_6I_8(C{\equiv}CC(O)OMe)_6]^{2-}$, the First Complex with Exclusively Organometallic Outer Ligands in the Family of Octahedral $\{M_6X_8\}$ Clusters

Maxim N. Sokolov,* Maxim A. Mikhailov, Konstantin A. Brylev, Alexander V. Virovets, Cristian Vicent, Nikolay B. Kompankov, Noboru Kitamura, and Vladimir P. Fedin

Reaction of $[Mo_6I_{14}]^{2-}$ with $HC{\equiv}CC(O)OMe$ in the presence of Ag^+ and Et_3N yielded the luminescent complex $[Mo_6I_8(C{\equiv}CC(O)OMe)_6]^{2-}$, the first fully organometallic complex in the family of octahedral $\{M_6X_8\}$ clusters. The cluster was crystallized as a tetraphenylphosphonium salt and characterized by X-ray single-crystal diffraction, elemental analysis, mass spectrometry, ^{13}C NMR, UV–vis, and luminescence spectroscopies.

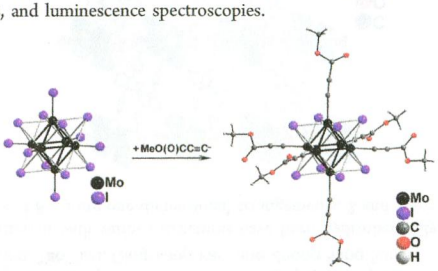

12482 dx.doi.org/10.1021/ic401491y

Polar and Magnetic Layered A-Site and Rock Salt B-Site-Ordered $NaLnFeWO_6$ (Ln = La, Nd) Perovskites

M. Retuerto, M. R. Li, A. Ignatov, M. Croft, K. V. Ramanujachary, S. Chi, J. P. Hodges, W. Dachraoui, J. Hadermann, T. Thao Tran, P. Shiv Halasyamani, C. P. Grams, J. Hemberger, and M. Greenblatt*

We synthesized and characterized $NaLaFeWO_6$ and $NaNdFeWO_6$ double perovskites with the unusual combination of layered order in the A sublattice and rock salt order over the B sublattice and determined that the compounds are monoclinic with noncentrosymmetric, $P2_1$ space group. The materials are ordered antiferromagnetically below $T_N \approx 25$ K. The magnetic structure of $NaNdFeWO_6$ has been solved with a propagation vector of $k = (^1/_2\ 0\ ^1/_2)$, and both Fe and Nd magnetic sublattices are antiferromagnetically ordered. The compounds are potentially multiferroic, but both denote the absence of a ferroelectric phase transition in the investigated temperature regime.

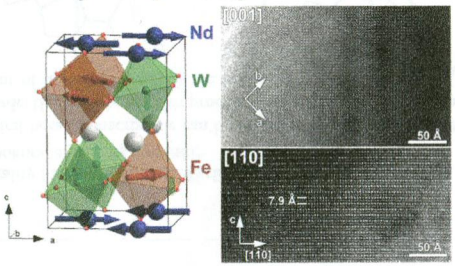

12492 dx.doi.org/10.1021/ic4014976

Synthesis of Phosphonic Acid Derivatized Bipyridine Ligands and Their Ruthenium Complexes

Michael R. Norris, Javier J. Concepcion, Christopher R. K. Glasson, Zhen Fang, Alexander M. Lapides, Dennis L. Ashford, Joseph L. Templeton, and Thomas J. Meyer*

We report here the efficient synthesis of 4,4′-bis(diethylphosphonomethyl)-2,2′-bipyridine and 4,4′-bis(diethylphosphonate)-2,2′-bipyridine, as well as the mono-, bis-, and tris-substituted ruthenium complexes. Access to these ligands and complexes in synthetically scalable ways is important to current research efforts for solar energy conversion.

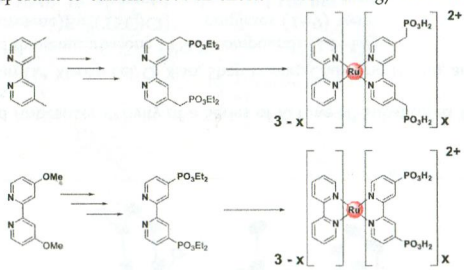

12502 S dx.doi.org/10.1021/ic401580y

Polyclusters and Substitution Effects in the Na–Au–Ga System: Remarkable Sodium Bonding Characteristics in Polar Intermetallics

Volodymyr Smetana, Gordon J. Miller, and John D. Corbett*

The clathrate-like sodium network in the structure of $Na_{1.0}Au_{0.18}Ga_{1.80}$.

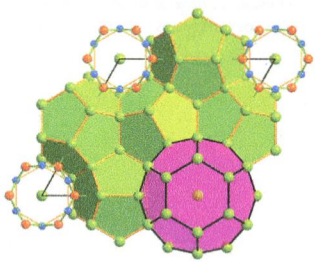

12511 S dx.doi.org/10.1021/ic401581q

Modulating Stepwise Photochromism in Platinum(II) Complexes with Dual Dithienylethene–Acetylides by a Progressive Red Shift of Ring-Closure Absorption

Bin Li, Hui-Min Wen, Jin-Yun Wang, Lin-Xi Shi, and Zhong-Ning Chen*

Stepwise photochromism in *trans*-platinum(II) complexes is increasingly facilitated with a progressive red shift of ring-closed absorption at dithienylethene units, ascribed to gradually enhanced transition character involving LUMO+1.

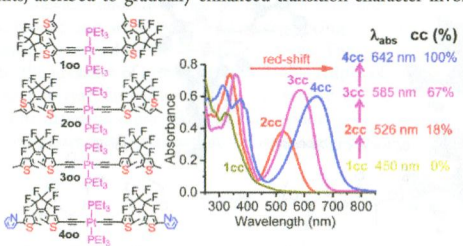

12521 S dx.doi.org/10.1021/ic401569n

New Supramolecular Au^{I}–Cu^{I} Complex as Potential Luminescent Label for Proteins

D. V. Krupenya, P. A. Snegurov, E. V. Grachova, V. V. Gurzhiy, S. P. Tunik,* A. S. Melnikov, P. Yu. Serdobintsev, E. G. Vlakh, E. S. Sinitsyna, and T. B. Tennikova*

Covalent adducts of human serum albumin (HSA), rabbit anti-HSA antibodies, and soybean trypsin inhibitor with a heterometallic gold–copper complex were synthesized and characterized. The complex, which is an extremely bright triplet emitter, under both one- and two-photon excitation, keeps its unique photophysical characteristics in the adducts, indicating the possibility for use of these conjugates as specific bioimaging reagents and in biochip technology.

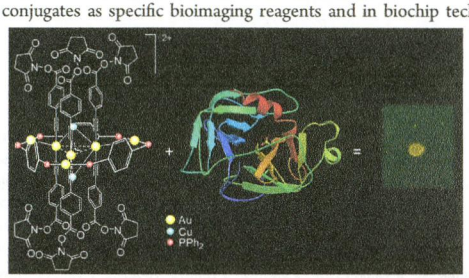

12529 dx.doi.org/10.1021/ic401615r

Electronic Structures and Magnetism of $SrFeO_2$ under Pressure: A First-Principles Study

Mavlanjan Rahman, Yao-zhuang Nie, and Guang-hua Guo*

At ambient pressure, the intralayer exchange interaction between $d_{x^2-y^2}$ orbitals of two adjacent Fe^{2+} ions through O p_σ is antiferromagnetic, as shown in at the left of the graphic; at high pressure, the intralayer exchange interaction between $d_{xz}d_{yz}$ orbitals of two adjacent Fe^{2+} ions through O p_π is ferromagnetic, as shown at the right.

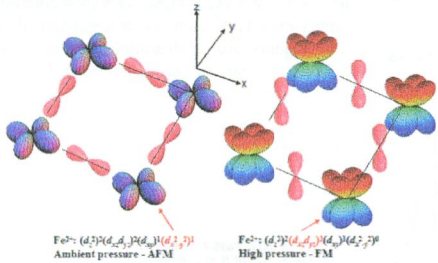

12535 S dx.doi.org/10.1021/ic4016228

Water-Soluble Co(III) Complexes of Substituted Phenanthrolines with Cell Selective Anticancer Activity

Sivaraman Jagadeesan, Vimalkumar Balasubramanian, Patric Baumann, Markus Neuburger, Daniel Häussinger, and Cornelia G. Palivan*

New water-soluble Co(III) complexes with methyl substituted phenanthroline ligands showed selective cytotoxicity with a significantly higher effect on intracellular mitochondrial function in PC-3 cells than in HeLa cells. The cytotoxicity of these complexes correlates to their hydrophobicity as an essential factor for high antitumor activity.

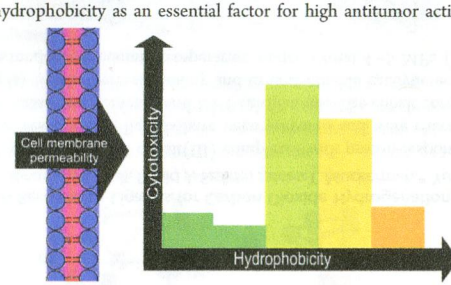

12545 S dx.doi.org/10.1021/ic401588j

***tert*-Butyl Hydroperoxide Oxygenation of Organic Sulfides Catalyzed by Diruthenium(II,III) Tetracarboxylates**

Leslie Villalobos, Julia E. Barker Paredes, Zhi Cao, and Tong Ren*

Diruthenium(II,III) tetracarboxylates efficiently catalyze the oxygenation of organic sulfides by *tert*-butyl hydroperoxide (TBHP). The study of linear free-energy relationships revealed the electrophilic nature of the diruthenium-activated peroxo species. Organic solubility of $Ru_2(esp)_2Cl$ enables catalytic reactions proceeding with high turnover frequency (TOF) and excellent selectivity under "solvent-free" conditions.

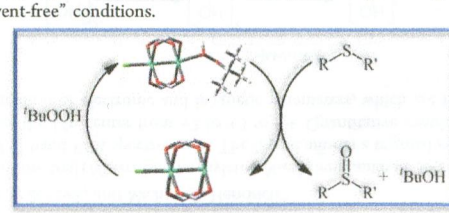

12553 S dx.doi.org/10.1021/ic4016367

Varying Substituents and Solvents To Maximize the Luminescence from [Ru(trpy)(bpy)CN]$^+$ Derivatives

Matthew A. Bork, Hunter B. Vibbert, David J. Stewart, Phillip E. Fanwick, and David R. McMillin*

The goal of this work has been to design luminescent forms with practicable emission quantum yields, and the focus has been on [Ru(X-T)(dmeb)CN]$^+$ systems, where X-T denotes 2,2′:6′,2″-terpyridine bearing substituent X at the 4′-position and dmeb denotes [2,2′-bipyridine]-4,4′-dicarboxylic acid, dimethyl ester. Results show that varying the π-electron-donating ability of the 4′-X substituent is an effective way to tune the energy and lifetime of the charge-transfer emission.

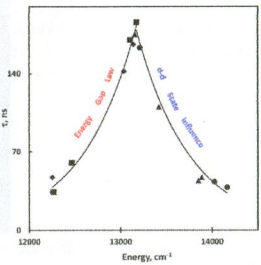

12561 S dx.doi.org/10.1021/ic4016756

8-Quinolinolato Gallium Complexes: Iso-selective Initiators for *rac*-Lactide Polymerization

Clare Bakewell, Andrew J. P. White, Nicholas J. Long,* and Charlotte K. Williams*

A series of gallium complexes, bearing 8-quinolinolato ligands, have been synthesized and are related to a series of aluminum complexes already reported. The complexes were found to be active in the ring-opening polymerization of *rac*-lactide at elevated temperatures (347 K). The 8-quinolinolato gallium complexes show improved rates, as compared to their aluminum analogues, and in some cases maintain a good degree of iso-selectivity.

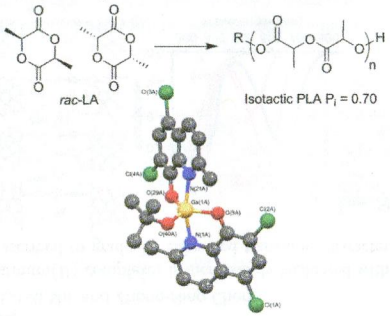

12568 dx.doi.org/10.1021/ic401681r

Characterization of Monomeric $Mn^{II/III/IV}$–Hydroxo Complexes from X- and Q-Band Dual Mode Electron Paramagnetic Resonance (EPR) Spectroscopy

Rupal Gupta, Taketo Taguchi, A. S. Borovik, and Michael P. Hendrich*

A series of Mn–OH complexes of the tris[(*N*′-*tert*-butylureaylato)-*N*-ethylene]aminato ligand were characterized with parallel and perpendicular mode, X- and Q-band EPR spectroscopy. The ligand affords a trigonal symmetry to the metal ion which is conserved during the oxidation of the Mn center from +2 to +3 to +4. Quantitative simulation of the electron paramagnetic resonance spectra allow determination of electronic and magnetic parameters, which are then compared with density functional calculations.

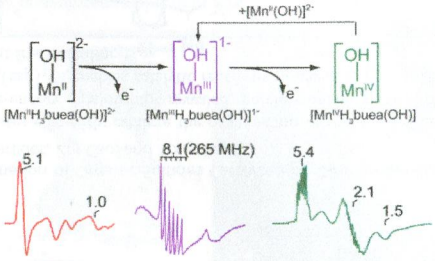

12576 dx.doi.org/10.1021/ic401707u

Cp*Co(III) Catalysts with Proton-Responsive Ligands for Carbon Dioxide Hydrogenation in Aqueous Media

Yosra M. Badiei, Wan-Hui Wang, Jonathan F. Hull, David J. Szalda, James T. Muckerman,* Yuichiro Himeda,* and Etsuko Fujita*

New water-soluble pentamethylcyclopendadienyl cobalt(III) complexes with proton-responsive 4,4′- and 6,6′-dihydroxy-2,2′-bipyridine (4DHBP and 6DHBP, respectively) ligands have been prepared and were characterized by X-ray crystallography, UV–vis and NMR spectroscopy, mass spectrometry, and DFT calculations. The cobalt complexes containing 4DHBP ligands ($[\mathbf{1}\text{–}\mathbf{OH_2}]^{2+}$ and $[\mathbf{1}\text{–}\mathbf{Cl}]^{+}$) display better thermal stability and exhibit notable catalytic activity for CO_2 hydrogenation to formate in aqueous bicarbonate media at moderate temperature under a total 4–5 MPa (CO_2:H_2 1:1) pressure.

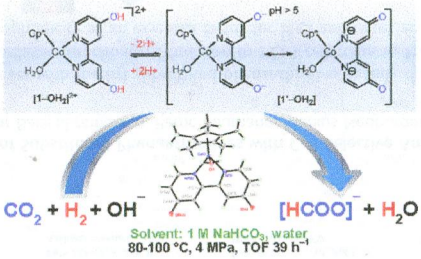

12587 S dx.doi.org/10.1021/ic401736f

Tris(3,5-di-*tert*-butylcatecholato)molybdenum(VI): Lewis Acidity and Nonclassical Oxygen Atom Transfer Reactions

Amanda H. Randolph, Nicholas J. Seewald, Karl Rickert, and and Seth N. Brown*

Tris(3,5-di-*tert*-butylcatecholato)molybdenum(VI) is Lewis acidic, forming a seven-coordinate dimer and isolable monomeric adducts with Lewis bases. It abstracts an oxygen atom from pyridine-*N*-oxide by a nonclassical mechanism, with autocatalysis originating from the similar reactivity of the bis(catecholate) complex initially produced in the reaction. Dioxygen also reacts, but forms some extradiol oxidation products in addition to the 1,2-benzoquinone.

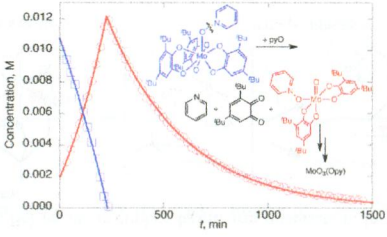

12599 S dx.doi.org/10.1021/ic401749q

Triangular Exchange Interaction Patterns in $K_3Fe_6F_{19}$: An Iron Potassium Fluoride with a Complex Tungsten Bronze Related Structure

Francesco Mezzadri,* Gianluca Calestani, Lara Righi, Chiara Pernechele, Massimo Solzi, and Clemens Ritter

$K_3Fe_6F_{19}$ is a charge ordered iron potassium fluoride showing a complex structure related to the tetragonal tungsten bronze one, with the perovskite cage being substituted by large S-shaped channels occupied by two potassium atoms. The magnetic structure is dominated by the presence of interconnected double stripes of antiferromagnetic triangular exchange interaction patterns alternately rotated in clock- and anticlockwise fashion. The magnetic order takes place in a wide temperature range, by increasing progressively the interaction dimensionality.

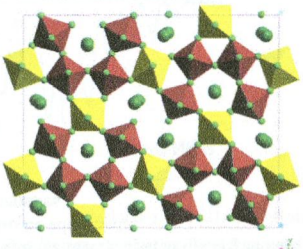

12605 dx.doi.org/10.1021/ic401757z

^{31}P Magic Angle Spinning NMR Study of Flux-Grown Rare-Earth Element Orthophosphate (Monazite/Xenotime) Solid Solutions: Evidence of Random Cation Distribution from Paramagnetically Shifted NMR Resonances

Aaron C. Palke,* Jonathan F. Stebbins, and Lynn A. Boatner

^{31}P magic angle spinning nuclear magnetic resonance spectra were collected on a series of flux-grown solid solutions of $La_{1-x}Ce_xPO_4$ (x between 0.027 and 0.32) having the monoclinic monazite structure, and of $Y_{1-x}M_xPO_4$ (M = V^{n+}, Ce^{3+}, Nd^{3+}, x between 0.001 and 0.014) having the tetragonal zircon structure. Paramagnetically shifted NMR resonances were used to ascertain information concerning solid solution mechanisms and local structural distortion caused by substitution of dissimilarly sized cations.

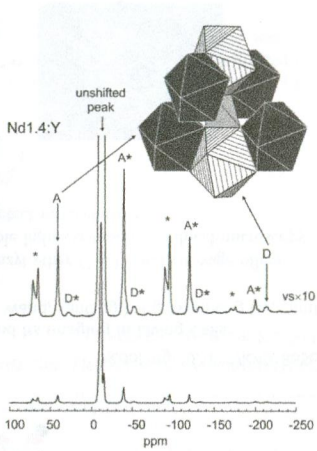

12616 S dx.doi.org/10.1021/ic401798b

Interaction between a Transition-Metal Fluoride and a Transition-Metal Hydride: Water-Mediated Hydrofluoric Acid Evolution Following Fluoride Solvation

Michele R. Chierotti, Andrea Rossin, Roberto Gobetto,* and Maurizio Peruzzini*

The reaction between the nickel(II) PCP pincer fluoride complex (^{tBu}PCP)Ni(F) and the tungsten(II) carbonyl hydride CpW(H)$(CO)_3$ leads to hydrogen fluoride formation, along with the bimetallic compound [CpW$(CO)_2$(μ-κ,C:κ,O-CO)Ni(^{tBu}PCP)]. The fluoride–hydride interaction is not direct but water-mediated, different from that found for the related hydride–hydride pair. The process has been studied through multinuclear ^{19}F, ^{31}P, and ^{1}H NMR spectroscopy combined with density functional theory calculations, at the M06//6-31+G(d,p) level of theory.

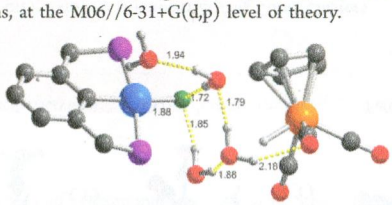

12624 S dx.doi.org/10.1021/ic4017855

Control of the Charge Distribution and Modulation of the Class II–III Transition in Weakly Coupled Mo_2–Mo_2 Systems

Xuan Xiao, Chun Y. Liu,* Qiao He, Mei Juan Han, Miao Meng, Hao Lei, and Xin Lu*

In weakly coupled Mo_2–Mo_2 systems, successive thiolation of the terephthalate bridge results in a class II–III transition, and structural nonsymmetry leads to the asymmetrical electrochemical and spectroscopic behaviors.

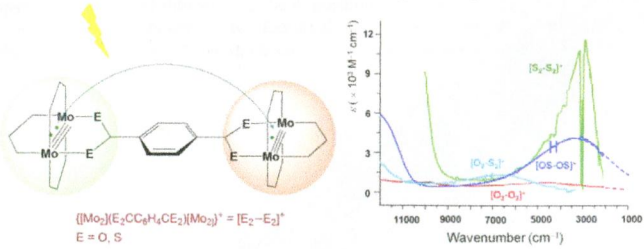

12634 S dx.doi.org/10.1021/ic401830f

Paramagnetic Hexacyanometalates. The Diversity of Spin Distribution Studied by ^{13}C and ^{15}N MAS NMR Spectroscopy

Natalia Baumgärtel, Alexandrine Flambard, Frank H. Köhler,* and Rodrigue Lescouëzec

The isotropic and anisotropic spin densities at the ligands of seven magnetic building blocks for molecular materials, $[M(CN)_6]^{n-}$, M = Cr, Mn, or Fe, have been determined after recording their solid-state ^{13}C and ^{15}N NMR spectra. The spin in the carbon and nitrogen 2s orbitals is negative and positive, respectively, in accord with the theory. Spin in the $2p_\pi$ and $2p_\sigma$ orbitals, crystal disorder, structural distortion, and scatter of the spin density have also be addressed.

Road map for molecular magnetism: NMR-detected spin densities

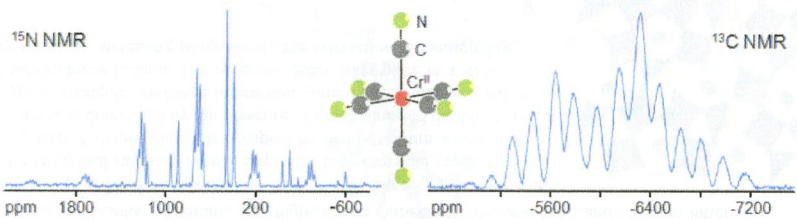

12645 S dx.doi.org/10.1021/ic401835d

Triphos Iridium(III) Halide Complex Photochemistry: Triphos Arm Dissociation

Andreas Ross and Paul R. Sharp*

Photolysis of Ir(triphos)X_3 (X = Cl, Br) results in triphos ligand arm dissociation. In the absence of trapping ligands, the unsaturated intermediate oligomerizes.

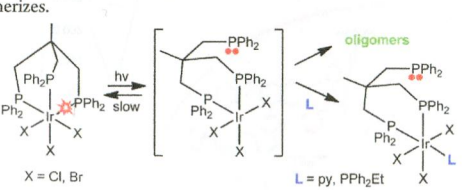

12655 S dx.doi.org/10.1021/ic401836n

Light-Enhanced Displacement of Methyl Acrylate from Iron Carbonyl: Investigation of the Reactive Intermediate via Rapid-Scan Fourier Transform Infrared and Computational Studies

Sohail Muhammad, Salvador Moncho, Bo Li, Samuel J. Kyran, Edward N. Brothers, Donald J. Darensbourg,* and Ashfaq A. Bengali*

Thermal displacement of methyl acrylate from $Fe(CO)_4(\eta^2\text{-}CH_2{=}CHCOOMe)$ by phosphine ligands is a slow process requiring hours at elevated temperatures. It is reported herein that photolysis of the tetracarbonyl complex with UV radiation greatly accelerates the process, where the reaction is complete in a few seconds. The release of methyl acrylate from this photochemically generated intermediate was shown to have a low barrier of 8.7 kcal/mol. DFT calculations were in good agreement with this experimental observation.

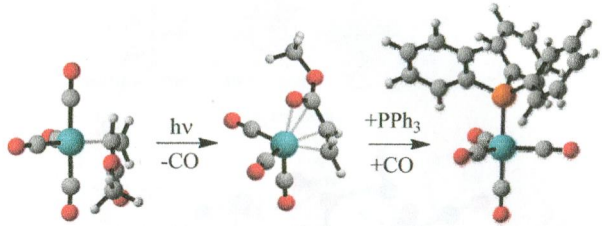

12661 S dx.doi.org/10.1021/ic4018536

Metal–Organic Frameworks Based on Previously Unknown Zr_8/Hf_8 Cubic Clusters

Dawei Feng, Hai-Long Jiang, Ying-Pin Chen, Zhi-Yuan Gu, Zhangwen Wei, and Hong-Cai Zhou*

The ongoing study of zirconium– and hafnium–porphyrinic metal–organic frameworks (MOFs) led to the discovery of isostructural MOFs based on Zr_8 and Hf_8 cubic clusters, which are known in neither cluster nor MOF chemistry. The MOFs exhibit high surface areas and gas uptakes and display very high catalytic selectivity for cyclohexane oxidation.

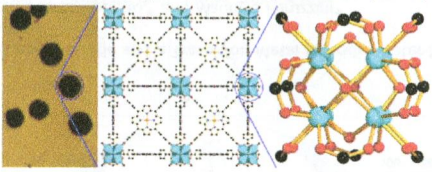

12668 S dx.doi.org/10.1021/ic401865e

A Highly Selective Fluorescence "Turn-On" Probe for Cu(II) Based on Reaction and Its Imaging in Living Cells

Zhaohua Shi, Xiaoliang Tang, Xiaoyan Zhou, Ju Cheng, Qingxin Han, Ji-an Zhou, Bei Wang, Yanfang Yang, Weisheng Liu,* and Decheng Bai*

A novel reaction-based Cu^{II} probe was designed and synthesized. Cu-mediated benzyl ether C–O bond cleavage offers excellent selectivity and turn-on fluorescent response in aqueous media under visible light excitation. Confocal microscopy experiments have demonstrated that the probe is membrane permeable and can detect intracellular Cu^{II}.

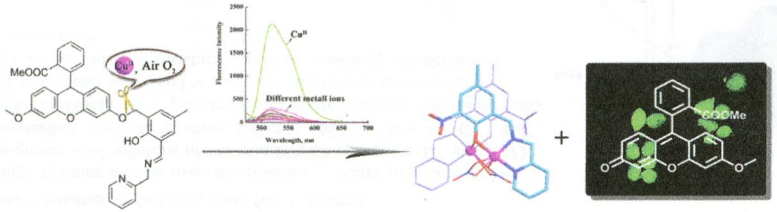

12674 S dx.doi.org/10.1021/ic4018773

Synthesis and Reactivity of New Bis(N-heterocyclic carbene) Iridium(I) Complexes

David J. Nelson, Byron J. Truscott, Alexandra M. Z. Slawin, and Steven P. Nolan*

Five new complexes of the form $[IrCl(\eta^2\text{-COE})(NHC)_2]$ are reported (COE = *cis*-cyclooctene; NHC = N-heterocyclic carbene). Reaction with CO allowed the preparation of the first structural analogue of Vaska's complex $[IrCl(CO)(PPh_3)_2]$ that bears two NHC ligands in place of two phosphines; the reactivity of this species was probed.

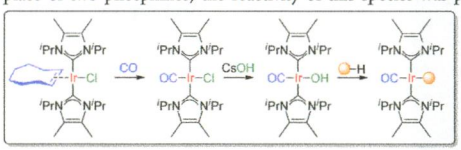

12682 S dx.doi.org/10.1021/ic401887b

Electron-Deficient Ternary and Quaternary Pnictides $Rb_4Zn_7As_7$, $Rb_4Mn_{3.5}Zn_{3.5}Sb_7$, $Rb_7Mn_{12}Sb_{12}$, and $Rb_7Mn_4Cd_8Sb_{12}$ with Corrugated Anionic Layers

Mansura Khatun, Stanislav S. Stoyko, and Arthur Mar*

Metal-centered tetrahedra and squre pyramids share edges to form corrugated anionic layers in the $Rb_4Zn_7As_7$- and $Rb_7Mn_{12}Sb_{12}$-type structures.

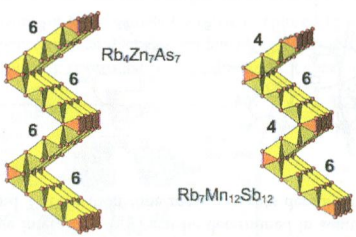

12691 S dx.doi.org/10.1021/ic401915b

Heteroscorpionate Magnesium Alkyls Bearing Unprecedented Apical σ-C(sp^3)–Mg Bonds: Heteroselective Ring-Opening Polymerization of *rac*-Lactide

Andrés Garcés, Luis F. Sánchez-Barba,* Juan Fernández-Baeza, Antonio Otero,* Manuel Honrado, Agustín Lara-Sánchez, and Ana M. Rodríguez

Different order nuclearity heteroscorpionate magnesium alkyls can be prepared by the reaction of the low sterically hindered acetamidinates $[Li(\kappa^3\text{-NNN})(THF)]$ with a series of RMgCl and subsequent reaction with 2 additional equivalents of the same Grignard reagent. The reaction in tetrahydrofuran gave rise to the dinuclear heteroscorpionate magnesium dialkyls $[RMg(\kappa^3\text{-}N,N,N;\kappa^2\text{-}C,N)MgR(thf)]$, whereas in the presence of dioxane, analogous tetranuclear tetraalkyls $[\{RMg(\kappa^3\text{-}N,N,N;\kappa^2\text{-}C,N)MgR\}_2\{\mu\text{-}O,O\text{-}(C_4H_8)\}]$ were obtained.

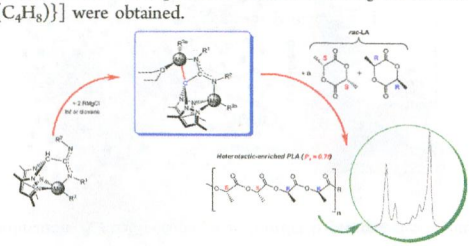

12702 S dx.doi.org/10.1021/ic4019184

The Effect of Specific Solvent–Solute Interactions on Complexation of Alkali-Metal Cations by a Lower-Rim Calix[4]arene Amide Derivative

Gordan Horvat, Vladimir Stilinović, Branko Kaitner, Leo Frkanec, and Vladislav Tomišić*

An interesting inclusion of a benzonitrile molecule in the hydrophobic cavity of the calixarene **L** complex with Li^+ was observed in the solid-state structure and by molecular dynamics simulations. Lithium cation was found to be coordinated by the PhCN nitrile group, and this interaction considerably enhanced the stability of the complex in solution, as evidenced by the results of thermodynamic investigations.

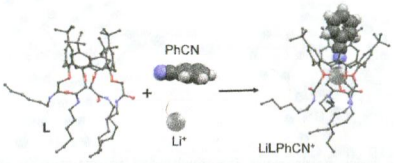

12713 S dx.doi.org/10.1021/ic4019212

Functionalized Bis-Cyclometalated Alkynylgold(III) Complexes: Synthesis, Characterization, Electrochemistry, Photophysics, Photochemistry, and Electroluminescence Studies

Vonika Ka-Man Au, Daniel Ping-Kuen Tsang, Keith Man-Chung Wong, Mei-Yee Chan,* Nianyong Zhu, and Vivian Wing-Wah Yam*

A series of luminescent gold(III) alkynyls, [Au(R-C^N^C)(C≡C—C_6H_4-R′)], has been synthesized and characterized. Tunable photoluminescence behaviors have been observed, with the solution emission maxima spanning through the visible region from 476 to 669 nm at room temperature. Selected complexes have been incorporated into the emissive layer of OLEDs and have demonstrated interesting electroluminescence.

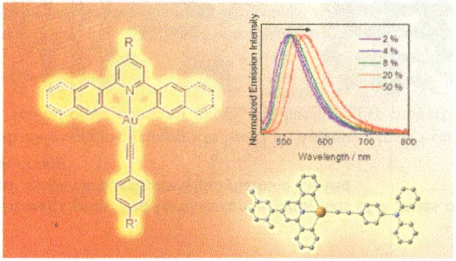

12726 S dx.doi.org/10.1021/ic402274s

From an Open Framework to a Layered and a Hexagonal Tungsten Oxide Structure: Controlled Transformation Reactions of an Extended Solid-State Material, $Cs_3Ga_7(SeO_3)_{12}$ to $Ga(OH)(SeO_3)$ and $KGa_3(SeO_4)_2(OH)_6$

Hyun Sun Ahn, Dong Woo Lee, and Kang Min Ok*

A highly symmetric open-framwork selenite, $Cs_3Ga_7(SeO_3)_{12}$, can be transformed to $Ga(OH)(SeO_3)$ with a layered structure and $KGa_3(SeO_4)_2(OH)_6$ having a hexagonal tungsten oxide (HTO) topology under mild conditions in a controlled manner.

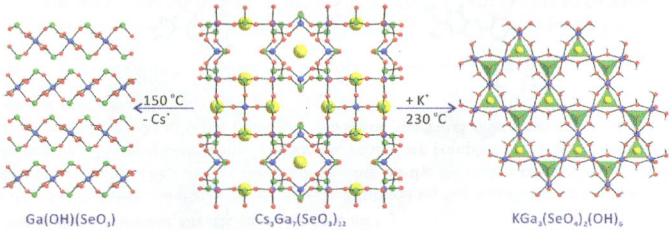

12731 dx.doi.org/10.1021/ic4019844

Synthesis and Structural Characterization of $RE_7Zn_{21}Tt_2$ (RE = La–Nd; Tt = Ge, Sn, and Pb): New Structure Type Among the Polar Intermetallic Phases

Nian-Tzu Suen and Svilen Bobev*

Reported here are the crystal and electronic structures and magnetic properties of the new polar intermetallic phase $RE_7Zn_{21}Tt_2$ (RE = La–Nd; Tt = Ge, Sn, and Pb). Main structural features are the Zn_{17}-cluster and the atoms of the tetrel elements in trigonal planar coordination. A small occupational disorder is present, the origins of which are originating in the electronic structure.

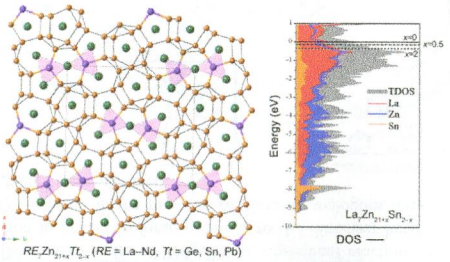

12741 dx.doi.org/10.1021/ic402016m

NMR Investigations of Dinuclear, Single-Anion Bridged Copper(II) Metallacycles: Structure and Antiferromagnetic Behavior in Solution

Daniel L. Reger,* Andrea E. Pascui, Perry J. Pellechia, and Andrew Ozarowski

Dinuclear copper(II) metallacycles containing single anion bridges have relatively sharp ^1H and ^{13}C NMR resonances with small hyperfine shifts due to the strong antiferromagnetic superexchange interactions. Variable-temperature NMR studies show the magnitude of the superexchage interaction ($-J$) can be determined in solution and coupled with two-dimensional (2D) NMR correlation spectroscopy and T_1 relaxation time measurements demonstrate that the solid-state structures are retained in solution.

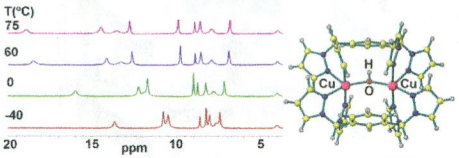

12749 dx.doi.org/10.1021/ic402017v

Dicyclopalladated Complexes of Asymmetrically Substituted Azobenzenes: Synthesis, Kinetics and Mechanisms

Marina Juribašić,* Ana Budimir, Snježana Kazazić, and Manda Ćurić*

Two series of new dicyclopalladated complexes of the 4,4′-disubstituted azobenzenes with varying substituents have been synthesized and fully characterized. The effect of these substituents on the formation rates of mono- and dicyclopalladated azobenzenes was studied by UV−vis spectroscopy. The kinetic results are complemented by the quantum-chemical calculations in order to provide insight into the possible mechanistic steps and rationalize experimental data as well as the substituent effects on the reaction rates.

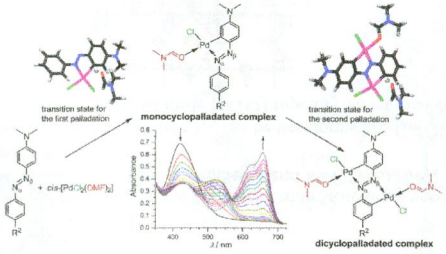

12758 dx.doi.org/10.1021/ic4020256

Gas Sorption, Second-Order Nonlinear Optics, and Luminescence Properties of a Series of Lanthanide−Organic Frameworks Based on Nanosized Tris((4-carboxyl)phenylduryl)amine Ligand

Yan-Ping He, Yan-Xi Tan, and Jian Zhang*

Presented here are a series of lanthanide−organic frameworks based on nanosized tris((4-carboxyl)phenylduryl)amine ligand, showing interesting gas sorption, second-order nonlinear optics, and luminescence properties.

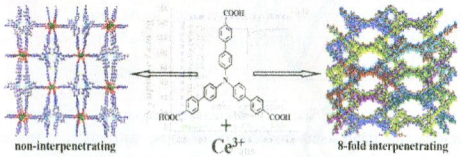

12763 dx.doi.org/10.1021/ic402037e

Molecular and Electronic Structures of Six-Coordinate "Low-Valent" $[M(^{Me}bpy)_3]^0$ (M = Ti, V, Cr, Mo) and $[M(tpy)_2]^0$ (M = Ti, V, Cr), and Seven-Coordinate $[MoF(^{Me}bpy)_3](PF_6)$ and $[MX(tpy)_2](PF_6)$ (M = Mo, X = Cl and M = W, X = F)

Mei Wang, Thomas Weyhermüller, Jason England, and Karl Wieghardt*

Neutral transition metal complexes $[M(bpy)_3]^0$ and $[M(tpy)_2]^0$ contain high-valent metal ions in highly reducing ligand environments consisting of π-radical monoanions $(bpy^{\bullet})^-$ and $(tpy^{\bullet})^-$, and/or the corresponding dianions $(bpy^{2-})^{2-}$ and $(tpy^{2-})^{2-}$. The oxidation level of these ligands can be experimentally determined using high resolution X-ray crystallography.

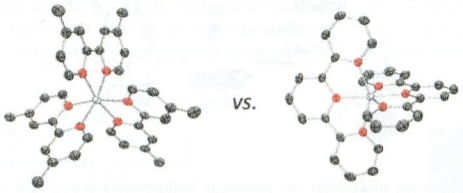

12777 S dx.doi.org/10.1021/ic4020477

Reversible Chemisorption of Sulfur Dioxide in a Spin Crossover Porous Coordination Polymer

Zulema Arcís-Castillo, Francisco J. Muñoz-Lara, M. Carmen Muñoz, Daniel Aravena, Ana B. Gaspar, Juan F. Sánchez-Royo, Eliseo Ruiz, Masaaki Ohba, Ryotaro Matsuda, Susumu Kitagawa, and José A. Real*

The spin crossover porous coordination polymer $\{Fe(pz)[Pt(CN)_4]\}$ reversibly chemisorbs SO_2 at room temperature. The chemisorption involves coordination of the SO_2 to Pt^{II} and stabilization of the Fe^{II} low-spin state.

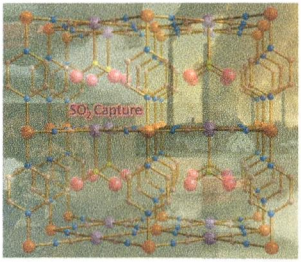

12784 S dx.doi.org/10.1021/ic402058f

Structural Dynamism and Controlled Chemical Blocking/Unblocking of Active Coordination Space of a Soft Porous Crystal

Abhijeet K. Chaudhari, Sanjog S. Nagarkar, Biplab Joarder, Soumya Mukherjee, and Sujit K. Ghosh*

Guest-dependent contraction and expansion of the channels have been explored by controlled chemical blocking and unblocking of a newly synthesized soft porous crystal. Detailed studies revealed up to 70% contraction of the void volume and almost a 100 times increase in gas sorption by controlled phases obtained by guest switching.

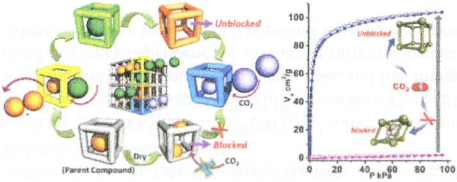

12790 S dx.doi.org/10.1021/ic402043x

New Polymorph of $InVO_4$: A High-Pressure Structure with Six-Coordinated Vanadium

Daniel Errandonea,* Oscar Gomis, Braulio García-Domene, Julio Pellicer-Porres, Vasundhara Katari, S. Nagabhusan Achary, Avesh K. Tyagi, and Catalin Popescu

Two HP phases are detected in $InVO_4$ by XRD and Raman spectroscopy. For one of them, found beyond 7 GPa, a wolframite-type structure is assigned. This HP phase implies a coordination change for *V*, whose coordination number is increased from 4 to 6. The phase transition involves changes in the electronic structure of $InVO_4$ causing a band gap collapse. The crystal structure of the different phases and the RT *P*–*V* equations of state are determined. Raman-active phonons are characterized for the different phases, and their pressure behavior is determined.

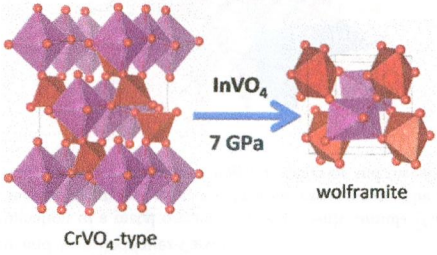

12799 S dx.doi.org/10.1021/ic402066h

Synthesis and Modular Structural Architectures of Mineralogically Inspired Novel Complex Pb Oxyhalides

Oleg I. Siidra,* Diana O. Zinyakhina, Anastasiya I. Zadoya, Sergey V. Krivovichev, and Rick W. Turner

Novel Pb oxyhalides have been prepared by high-temperature solid-state reactions and hydrothermal method. The new Pb oxyhalides are based upon novel $[O_{10}Pb_{20}]^{20+}$ (**1**) and $[O_{16}Pb_{22}]^{12+}$ (**2**) layers of edge- and corner-sharing oxocentered OPb_4 tetrahedra. The structure of **3** is the first example of the Pb oxyhalide with the 3:1 ratio between the O–Pb and X sheets. The structure topologies and architectures observed in these compounds are related to those observed in rare natural Pb oxyhalides.

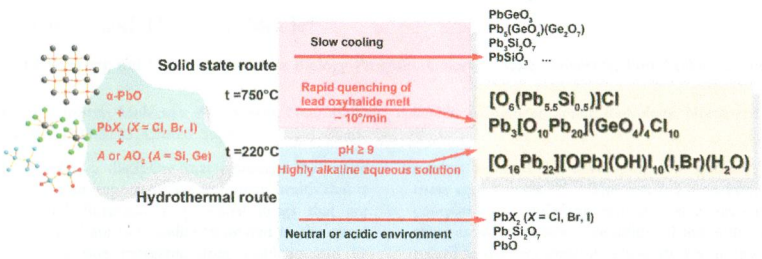

12806 dx.doi.org/10.1021/ic402069n

Oxygen Diffusion and Nonstoichiometry in $BiFeO_3$

Toshimitsu Ito,* Tomoharu Ushiyama, Mitsuko Aoki, Yasuhide Tomioka, Yukiya Hakuta, Hiroshi Takashima, and Ruiping Wang

We investigated the annealing process of stoichiometric $BiFeO_3$ grains in air and revealed that oxygen diffusion occurs in two steps: (1) the weight of the sample decreases in a short time, which originates from the generation of oxygen deficiency near the surface of the grains; and then (2) it increases gradually and slowly, which originates from oxygen diffusion toward equilibrium in the inner part of the grains, introducing excess oxygen there.

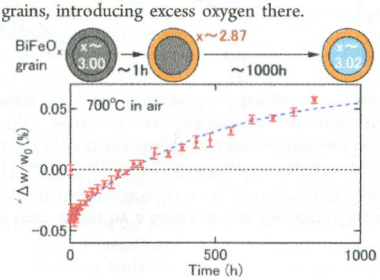

12811 dx.doi.org/10.1021/ic402152f

New Insights into Crystallite Size and Cell Parameters Correlation for ZnO Nanoparticles Obtained from Polyol-Mediated Synthesis

Isabelle Trenque, Stéphane Mornet, Etienne Duguet, and Manuel Gaudon*

A polyol-mediated synthesis has allowed the elaboration of ZnO nanocrystallites with controlled crystallite and aggregate sizes. Both *a* and *c* cell parameters increase while the crystallite size decreases. A simple model to fit this grain-surface relaxation was successfully developed.

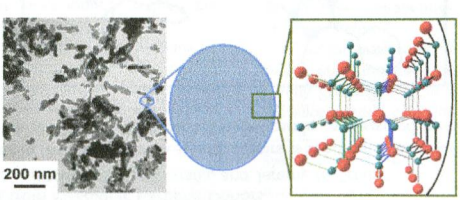

12818 (S) dx.doi.org/10.1021/ic402186p

Neutron Diffraction Studies of the Molecular Compound $[Co_2(bta)]_n$ (H_4bta =1,2,4,5-Benzenetetracarboxylic Acid): In the Quest of Canted Ferromagnetism

Oscar Fabelo,* Laura Cañadillas-Delgado, Jorge Pasán,* Pau Díaz-Gallifa, Catalina Ruiz-Pérez, Francesc Lloret, Miguel Julve, Inés Puente Orench, Javier Campo, and Juan Rodríguez-Carvajal

The full magnetic-structure determination of a metal organic framework with formula $[Co_2(bta)]_n$ has been performed by combining macroscopic magnetic measurements and neutron diffraction experiments. The presence of spontaneous and field-induced magnetic stacking faults is at the origin of the bulk magnetic behavior and the slow magnetic relaxation observed in this system.

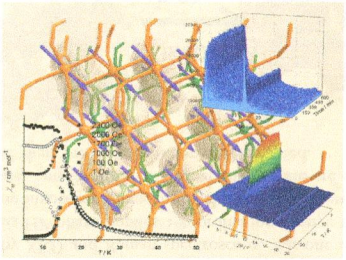

12828 (S) dx.doi.org/10.1021/ic4022273

Synthesis, Structure, Luminescent, and Magnetic Properties of Carbonato-Bridged $Zn^{II}_2Ln^{III}_2$ Complexes $[(\mu_4\text{-}CO_3)_2\{Zn^{II}L^nLn^{III}(NO_3)\}_2]$ (Ln^{III} = Gd^{III}, Tb^{III}, Dy^{III}; L^1 = *N,N′*-Bis(3-methoxy-2-oxybenzylidene)-1,3-propanediaminato, L^2 = *N,N′*-Bis(3-ethoxy-2-oxybenzylidene)-1,3-propanediaminato)

Kiyomi Ehama, Yusuke Ohmichi, Soichiro Sakamoto, Takeshi Fujinami, Naohide Matsumoto,* Naotaka Mochida, Takayuki Ishida, Yukinari Sunatsuki, Masanobu Tsuchimoto, and Nazzareno Re

Carbonato-bridged $Zn^{II}_2Ln^{III}_2$ complexes $[(\mu_4\text{-}CO_3)_2\{Zn^{II}L^nLn^{III}(NO_3)\}_2]$·solvent were synthesized through atmospheric CO_2 fixation. $Zn^{II}_2Gd^{III}_2$ complexes showed ferromagnetic Gd^{III}–Gd^{III} interaction. The Stark splitting of the ground state for $Zn^{II}_2Tb^{III}_2$ and $Zn^{II}_2Dy^{III}_2$ complexes was evaluated from the magnetic data, and the energy pattern indicates an easy-axis anisotropy. Those complexes showed frequency-dependence in alternating current magnetic susceptibility. The luminescence spectra of $Zn^{II}_2Tb^{III}_2$ complexes exhibited the fine structure of the ground state, being in accord with the energy pattern from the magnetic analysis.

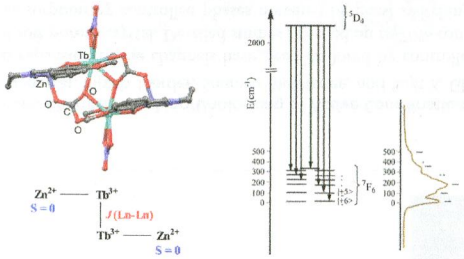

12842 Ⓢ dx.doi.org/10.1021/ic402311c

A Tripodal Ligand Constructed from Mesoionic Carbene Donors

Wei-Tsung Lee, Diane A. Dickie, Alejandro J. Metta-Magaña, and Jeremy M. Smith*

A tripodal ligand constructed solely from mesoionic carbene donors is reported. The donor strength of this ligand is lower than those for most imidazol-2-ylidene-based tris(carbene)borate ligands, as measured by IR spectroscopy of $\{NiNO\}^{10}$ and $\{Mn(CO)_3\}^+$ derivatives.

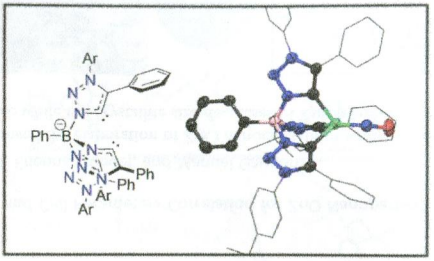

12847 Ⓢ dx.doi.org/10.1021/ic4023882

Electrocatalytic Hydrogen Evolution from Water by a Series of Iron Carbonyl Clusters

An D. Nguyen, M. Diego Rail, Maheswaran Shanmugam, James C. Fettinger, and Louise A. Berben*

A series of low-valent iron clusters, $[Fe_4N(CO)_{12}]^-$, $[Fe_4C(CO)_{12}]^{2-}$, $[Fe_5C(CO)_{15}]^{2-}$, and $[Fe_6C(CO)_{18}]^{2-}$, catalyze hydrogen evolution from water at pH 5. The butterfly-shaped four-iron clusters are best able to stabilize hydride intermediates and to produce hydrogen. $[Fe_4N(CO)_{12}]^-$ works via successive electron and proton transfers while $[Fe_4C(CO)_{12}]^{2-}$ operates via two proton-coupled electron transfer steps. We attribute the difference in mechanism to the different charges on the clusters.

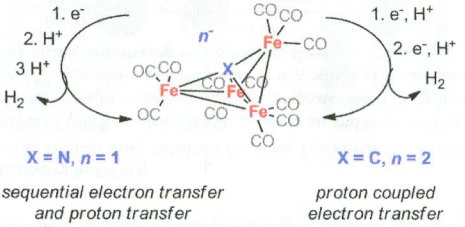

Ⓢ Supporting Information available via online article